Modeling and Control of Variable Speed Drive Based Loads for Grid Primary Frequency Support

Shuyao Wang, *Member, IEEE*, Yiwei Ma, *Member, IEEE*, Kaiqi Sun, *Member, IEEE*, Jingxin Wang, *Member, IEEE*, Hongyu Li, *Student Member, IEEE*, Leon M. Tolbert, *Fellow, IEEE*, and Fred Wang, *Fellow, IEEE*

***Abstract*—The amount of electricity generation from renewable energy resources (RES) has been increasing significantly all over the globe. However, traditional power grid management is challenged when a large amount of intermittent and unpredictable RES-based generation units are integrated into the power network. This can lead to more severe grid frequency fluctuation events. In this paper, a variable speed drive (VSD) based motor load is utilized as a frequency responsive load to support grid frequency stability. A primary frequency control scheme is proposed and applied to the VSD-based motor load, which incorporates the sophisticated rotating speed feedback controller. Additionally, the proposed frequency responsive VSD-based load is modeled and simplified. As a result, a droop-like response can be achieved with multiple VSD load units. The effectiveness of the proposed model and control scheme is evaluated by experimental studies performed in a multi-converter-based hardware testbed (HTB).**

***Index Terms*—Aggregated model, droop control, hardware testbed, primary frequency control, variable speed drive.**

I. Introduction

NOWADAYS, the amount of electricity generation from renewable energy resources (RES) has been dramatically increasing all over the globe. According to [1], renewable electricity generation is expected to increase to 38% of the total electricity generation by 2050. The vast integration of RES into the electric power grid imposes great challenges to the traditional centralized management system due to its intermittence and unpredictability, which causes more severe grid frequency fluctuation events [2], [3], [4].

Conventionally, grid frequency regulation is mainly provided by synchronous generator (SG) primary frequency control, which aims to balance generation and load demand [5]. However, due to difficulties introduced by intermittent RES, it is more expensive and technically complex to guarantee grid stability and reliability by only using the conventional regulation scheme provided by SGs. Therefore, the concept of using fast-response non-critical loads to support the grid frequency has emerged in recent research. As proposed in [6], [7], [8], non-critical loads can tolerate a wide range of variation in the supply voltage magnitude and frequency, so it is suitable to be utilized for providing grid frequency support. Meanwhile, using non-critical loads as grid power reserve is more economical than only using energy storage units as power reserve [9], [10], [11], [12], since less energy storage capacity will be required [13], [14].

A. Frequency Responsive Load

Induction motors are one category of the most commonly used loads for frequency support, since non-critical motor loads, such as pumps and fans for ventilation and temperature regulation, can temporarily adjust their rotating speed without affecting the corresponding primary process goal [15]. Meanwhile, motor loads account for a large amount of the total load power consumption, so they can provide sufficient grid power reserve in many instances. Variable speed drives (VSDs) have been widely applied to control induction motors considering the benefits of performance improvement and overall energy savings. In addition, a motor driven by a VSD can be directly used for grid support by implementing control schemes to the motor drive without installing any extra power electronics (PE) interfaces. So, VSD-based loads are regarded as promising candidates for responsive loads. Meanwhile, the VSD-based load reliability after grid power outages can be improved by applying the specific control algorithm to the PE interface. In this paper, VSD motor load will be referred to as "VSD load" in the following paragraphs for simplicity consideration.

However, there are still research gaps regarding the load modeling and frequency control design in using multiple VSD loads for grid frequency regulation. First, there is a lack of

Manuscript received 8 March 2022; revised 3 June 2022 and 31 July 2022; accepted 10 September 2022. Date of publication 30 September 2022; date of current version 24 March 2023. This work was supported in part by the Engineering Research Center Program of the National Science Foundation and the Department of Energy under NSF Award EEC-1041877 and in part by the CURENT Industry Partnership Program. Paper no. TPWRD-00298-2022. *(Corresponding author: Shuyao Wang.)*

Shuyao Wang, Jingxin Wang, Hongyu Li, and Leon M. Tolbert are with the Department of Electrical Engineering and Computer Science, The University of Tennessee, Knoxville, TN 37996 USA (e-mail: swang67@vols.utk.edu; jwang78@utk.edu; hli90@utk.edu; tolbert@utk.edu).

Kaiqi Sun is with the Department of Electrical Engineering and Computer Science, The University of Tennessee, Knoxville, TN 37996 USA, and also with the School of Electrical Engineering, Shandong University, Jinan, China (e-mail: skq@sdu.edu.cn).

Yiwei Ma is with the Department of Electrical Engineering and Computer Science, The University of Tennessee, Knoxville, TN 37996 USA, and also with the Electric Power Research Institute, Knoxville, TN 37932 USA (e-mail: yma@epri.com).

Fred Wang is with the Department of Electrical Engineering and Computer Science, The University of Tennessee, Knoxville, TN 37996 USA. He is now with the Oak Ridge National Laboratory, Knoxville, TN 37932 USA (e-mail: fred.wang@utk.edu).

Color versions of one or more figures in this article are available at https://doi.org/10.1109/TPWRD.2022.3211181.

Digital Object Identifier 10.1109/TPWRD.2022.3211181

investigation on dynamic VSD load representation when providing grid support. For example, static electric elements are widely used to represent the load performance based on current research [16], [17], [18], which are not necessarily accurate enough for representing VSD loads.

Second, effective VSD load control is required for more advanced frequency support performance. VSD load frequency support approaches can be classified as: 1) regulating the load on/off status, or 2) regulating motor rotating speed. The first approach is proposed in [19], [20], [21], [22], which follows the principle that the grid frequency is regulated by turning off or on end-users according to a higher-level control plan. This approach features a simple and efficient control algorithm for each end-user. However, each load unit is required to adopt a discontinuous operation mode during the frequency event. Meanwhile, this approach requires an even distribution of the device dead-band frequency and nominal power to provide an appropriate frequency to power ($f-p$) droop response, which is a challenge considering the randomness of changing loads in the system.

In the second support approach, the grid frequency is regulated by motor rotating speed variation. As proposed in [23], [24], [25], the VSD power consumption reference is derived based on grid frequency variation following $f-p$ droop response. Afterward, the power reference will be transferred as a rotor speed command according to inherent motor load characteristics. However, only the induction motor open-loop control scheme, *i.e.,* the widely used constant volt-per-hertz (V/f) control, is adopted by the VSD load speed regulator based on existing research literature. The constant V/f control is cost-efficient since no sophisticated processor is required, but it also limits the VSD performance accuracy and control effectiveness. For example, an overshoot on the load power consumption is observed if the slew rate of the motor speed reference is large [23], [24], [25]. Meanwhile, the open-loop controller cannot accurately constrain the motor rotating speed since no speed feedback loop is applied [26]. Additionally, since the constant V/f controller is not suitable for the complicated computational process, it is not practical to incorporate the power − rotor speed transfer into the constant V/f VSD controller, as introduced in the control algorithm above. In literature [27], the control algorithm is simplified as directly transferring the grid frequency deviation to the motor rotating speed command deviation. However, only the grid frequency drop and recovery is discussed, without considering the VSD load support regarding grid frequency increase. Additionally, [27] did not provide a numerical model of VSD load with frequency support, which is less beneficial for flexible application in analytical studies, simulation and emulation cases.

B. Contributions

VSD load is suitable for providing grid frequency support considering the sufficient power reserve and flexible control application. However, there is still a lack of investigation on load modeling and control design. Therefore, the following aspects are emphasized in this paper:

1) Propose a primary frequency support control scheme based on industrial VSD loads, as well as a coordination strategy among multiple load units. An effective grid-frequency response mimicking the conventional droop-control can be provided.

2) Develop a simplified responsive VSD load model which highlights the proposed frequency support control scheme.

3) Experiments are performed to evaluate the proposed VSD load frequency support control strategy.

The article is organized as follows: Section II introduces the topology and control schemes of the VSD load studied in this paper, and a VSD simplified model is developed based on the introduced detailed load model. Section III explains the frequency support scheme applied to a single VSD load unit. Section IV proposes the coordination control between multiple VSD load units to provide the droop-like $f-p$ response for the grid frequency support control. Section V shows the experimental analysis of frequency support provided by VSD loads.

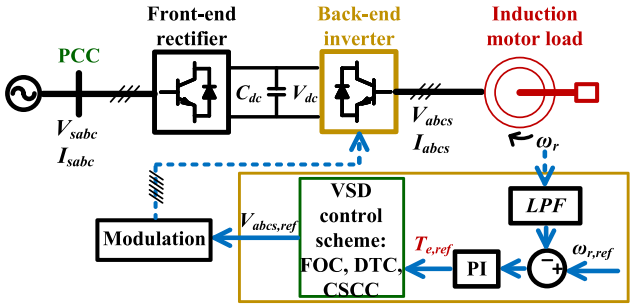

Fig. 1. VSD-based induction motor load configuration.

II. VSD Load Topology and Simplification

The simplified model of the VSD load unit with closed-loop speed controllers is introduced in this section, which will be used as the basis of the VSD load model.

A. VSD Load and Controller Model

The active front-end VSD load studied in this paper is illustrated in Fig. 1. The VSD load system includes a three-phase induction motor and a variable frequency power supply, consisting of a front-end rectifier and a back-end inverter.

In this article, the VSD load model is represented by the voltage source converter (VSC) dynamic average-value model, of which the dynamic performance is mainly decided by controllers embedded in back-end inverters, as well as some major passive electric components [28], [29]. Furthermore, frequently used closed-loop controllers are selected and modeled as an integral part of the VSD load, including field-oriented control (FOC), direct torque control (DTC), and constant slip current control (CSCC). Mathematical expressions of the above controllers can be found in [30].

B. VSD Load Simplified Model With Closed-Loop Control

The main principle of the three closed-loop controllers mentioned in the last subsection is to provide a torque transducer for which the electromagnetic torque T_e is instantaneously equal to the command $T_{e,ref}$. Meanwhile, closed-loop controllers drive the back-end inverter to provide the desired T_e, so motor drives with the aforementioned three control schemes demonstrate

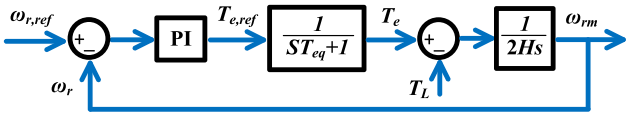

Fig. 2. VSD simplified model utilizing closed-loop control.

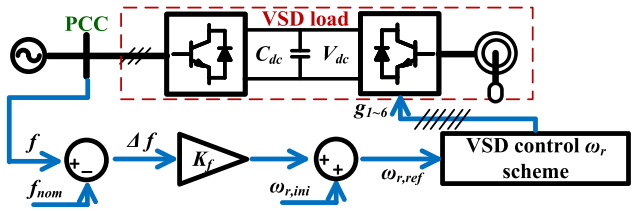

Fig. 3. VSD load frequency support control diagram.

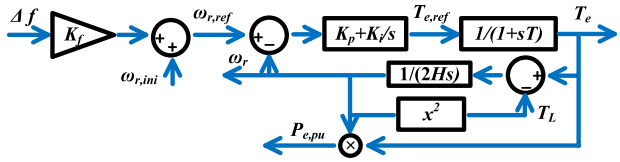

Fig. 4. VSD driving pump/fan loads with frequency control.

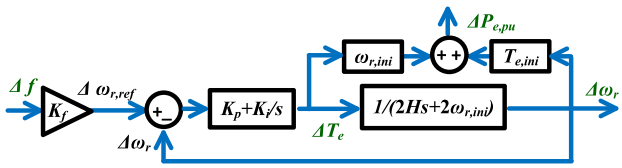

Fig. 5. Linearized model for the single VSD load unit.

similar dynamic characteristics if employing an identical motor speed controller. Therefore, the closed-loop VSD load can be simplified based on the following considerations:

1) The front-end rectifier provides a stable dc-link voltage which guarantees the regular operation of the following power stage. The extreme ac terminal voltage conditions, which include the excessive over-voltage and under-voltage at the load terminal, are not of consideration according to the research scope in this paper, since the model of VSD load with grid frequency support is no longer valid under these conditions.
2) The motor load reactive power consumption is provided by the dc-link capacitor C_{dc} from VSD back-to-back inverter, so the induction motor reactive power consumption is removed from the VSD load power consumption model.
3) Motor drive controller inner regulation loops, including the current control loop in FOC and CSCC, and the T_e control loop in DTC, can be simplified as time delay compared with the relatively slow-response control process.
4) The VSD load provides a relatively constant operating efficiency η_{VSD} over a wide operation range [31], [32]. So the total VSD power consumption is proportional to the rotating load power consumption.

According to the above considerations, a closed-loop VSD load simplified model in a p.u. system is illustrated in Fig. 2. Transferring $T_{e,ref}$ to T_e is simplified as a time delay considering the rapid response of the inner control loop and modulation process. The motor speed controller dynamic model is maintained in the simplified model to provide $T_{e,ref}$. Meanwhile, considering the induction motor characteristics, only the q-axis is modeled to reflect the motor load active power dynamic performance, while the d-axis is ignored since the reactive power is decoupled.

III. VSD Load Grid Frequency Support Control

A. VSD Load Grid Frequency Control Scheme

The VSD load grid frequency support based on $f-p$ droop response is introduced to precisely regulate the load power, which is illustrated in Fig. 3. For one VSD load unit, the grid frequency deviation Δf is measured at the point of common coupling (PCC). Rotor speed command $\omega_{r,ref}$ is generated with respect to Δf as expressed in (2):

$$\Delta f = f - f_{nom} \tag{1}$$

$$\omega_{r,ref} = K_f \cdot \Delta f + \omega_{r,ini} \tag{2}$$

When f decreases below nominal frequency f_{nom}, $\omega_{r,ref}$ will decrease proportional to Δf by K_f following (2). After the grid frequency is stabilized, ω_r is lower than the initial value $\omega_{r,ini}$ due to Δf and K_f, which decreases the VSD load consumption. This will help mitigate Δf when subjected to a grid disturbance, which is similar to the effect of conventional primary frequency control. The operating condition when f increases can be explained similarly. Additionally, coordinating multiple VSD loads to follow the $f-p$ droop curve will be explained later.

B. VSD Load Simplified Model With Grid Frequency Support

By decoupling the front-end and back-end PE interfaces, the VSD load dynamic performance can be expressed by the speed regulator and the torque-to-speed expression. So the simplified model of VSD loads with frequency support control is expressed as Fig. 4, combining the frequency regulation scheme in Fig. 3 and simplified VSD load model in Fig. 2. In Fig. 4, load torque T_L is represented by ω_r following $T_L = {\omega_r}^2$ considering the pump/fan type of load is studied in this paper. To maintain the controller system stability, the bandwidth of the internal control loop should be faster than the external control loop. The internal voltage and current control loop driven by $T_{e,ref}$ should be about 10 times faster than the external T_e loop which is driven by $\Delta\omega_r$.

Meanwhile, the motor drive closed-loop control and modulation are simplified as a time delay process, of which the time constant T_{eq} represents the T_e response time. This time delay process can be ignored, since the VSD back-end inverter response speed is much faster than the rest of the loops in the responsive VSD load model.

The VSD load linearized model is illustrated in Fig. 5 based on Fig. 4. The linearized model parameters include the controller

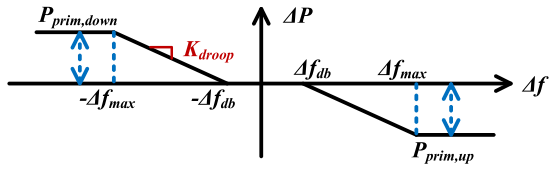

Fig. 6. $f-p$ droop control diagram.

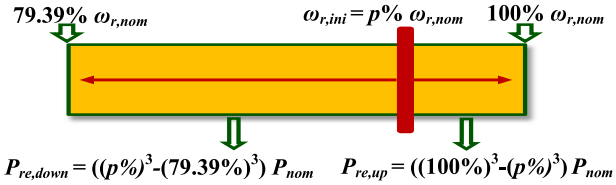

Fig. 7. Operational reserve provided by single VSD load unit.

parameters K_f, the T_e proportional-integrator (PI) controller parameters K_p, K_i, the initial variables $\omega_{r,ini}$, $T_{e,ini}$, and the motor load inertia constant H. The electric torque control loop response delay T_{eq} is removed for simplfying the VSD load model. The VSD power consumption deviation $\Delta P_{e,pu}$ linearized expression is proportional to ΔT_e and $\Delta\omega_r$:

$$\Delta P_{e,pu} = \Delta T_e \cdot \omega_{r,ini} + T_{e,ini} \cdot \Delta\omega_r \tag{3}$$

The VSD load transfer function can be expressed as (4) according to the VSD load linearized model in Fig. 5:

$$\frac{\Delta P_{e,pu}}{\Delta f} = \frac{a_2\, s^2 + a_1\, s + a_0}{b_2\, s^2 + b_1\, s + b_0} \tag{4}$$

Transfer function coefficients in (4), *i.e.*, a_2, a_1, a_0, b_2, b_1 and b_0, are expressed as:

$$b_2 = 2H \tag{5}$$

$$b_1 = 2\omega_{r,ini} + K_p \tag{6}$$

$$b_0 = K_i \tag{7}$$

$$a_2 = 2HK_fK_p\omega_{r,ini} \tag{8}$$

$$a_1 = K_f(2HK_i\omega_{r,ini} + 2\omega^2{}_{r,ini}K_p + T_{e,ini}K_p) \tag{9}$$

$$a_0 = K_fK_i(2\omega^2{}_{r,ini} + T_{e,ini}) \tag{10}$$

IV. VSD Load Potential Regarding Primary Frequency Support

Discussion of the VSD load frequency response is presented in this section, including the VSD load potential in terms of providing frequency support, and the coordination control scheme to provide frequency droop control based on multiple VSD loads.

A. f - p Droop Control

PE-based devices are usually regulated to follow the $f-p$ droop control, which mimic the SG governor to provide primary frequency response [33], [34], [35], [36], [37]. The SG output active power reference deviation ΔP_{ref} during the grid contingency is proportional to Δf by the predefined droop rate K_{droop} which is illustrated in Fig. 6 and expressed by (11).

$$\Delta P_{ref} = K_{droop}\Delta f \tag{11}$$

As shown in Fig. 6, Δf_{db} represents the deviation between dead-band frequency f_{db} and f_{nom}. f_{max} represents the frequency when all available power reserves are utilized for frequency support. Δf_{max} represents the deviation between f_{max} and f_{nom} as expressed in (12). $P_{prim,up}$ and $P_{prim,down}$ represent the maximum available power reserve in frequency increase or decrease.

$$\Delta f_{max} = f_{max} - f_{nom} \tag{12}$$

Generally, K_{droop} is determined based on Δf_{max} and P_{prim} as shown in (13). When grid frequency reaches f_{max}, all power reserve for primary frequency should be released. f_{db}, f_{max} are decided by central controller according to the regional frequency response obligation [38]. Considering Δf_{max} is a predefined constant value, K_{droop} is mainly determined by $P_{prim,up}$ and $P_{prim,down}$, which will be jointly represented as P_{prim} in the following passages.

$$K_{droop} = \frac{P_{prim}}{P_{base,sys}} \cdot \frac{1}{(\Delta f_{max} - \Delta f_{db})} \tag{13}$$

where $P_{base,sys}$ represents the grid power base.

B. Frequency Support Capacity of Individual VSD Load

The overload tolerance of different VSD load components varies significantly. For example, the motor can tolerate overload conditions for a relatively long time. In comparison, VSDs allow the current to stay between 100% and 150% of the nominal current for around 60 seconds [39]. Therefore, it is not recommended to run the VSD at overcurrent status constantly.

A VSD-driven pump/fan load can be adjusted actively by customers to achieve high operating efficiency under different operating conditions. As suggested in [40], the optimal operating speed of pump loads ranges from 80% to 100% nominal rotating speed $\omega_{r,nom}$. Therefore, the VSD load can provide a wide power adjustment range without overloading.

Accordingly, the available power reserve of an individual VSD load unit is defined in Fig. 7 considering electric devices tolerance and efficiency. Load units operating between 79.39% and 100% $\omega_{r,nom}$ are regarded as available to be utilized as responsive load, which is equivalent to between 50% and 100% P_{nom} for the pump/fan load, where P_{nom} denotes the VSD nominal power. Assuming that $\omega_{r,ini} = p\%\ \omega_{r,nom}$, the VSD load unit operational reserve is expressed as:

$$P_{re,down,i} = ((p\%)^3 - (79.39\%)^3) \cdot P_{nom} \tag{14}$$

$$P_{re,up,i} = ((100\%)^3 - (p\%)^3) \cdot P_{nom} \tag{15}$$

where $P_{re,down,i}$ represents downwards power reserve of i^{th} load unit for preventing grid frequency from decreasing, $P_{re,up,i}$ represents upwards power reserve for preventing the grid frequency from increasing.

C. Multiple VSD Loads Frequency Support Capacity

The total power reserve in p.u. value provided by multiple VSD load units at grid frequency increase and decrease events can be expressed as (16) and (17) according to the single load power reserve in (14) and (15):

$$P_{re,down,pu} = \frac{\sum_{i=1}^{n} P_{re,down,i}}{P_{base,sys}} \tag{16}$$

$$P_{re,up,pu} = \frac{\sum_{i=1}^{n} P_{re,up,i}}{P_{base,sys}} \tag{17}$$

where n represents the number of VSD load units available to participate in frequency regulation.

The primary frequency response droop rate is determined by $P_{prim,down}$ and $P_{prim,up}$ respectively, which should not exceed the limit of $P_{re,down}$ and $P_{re,up}$. Regardless of frequency deviation direction, assume the ratio between P_{prim} and P_{re} is expressed as:

$$K_{prim} = \frac{P_{prim,pu}}{P_{re,pu}} \tag{18}$$

Substitute (18) into (16) or (17), $P_{prim,pu}$ is expressed as:

$$P_{prim,pu} = \frac{\sum_{i=1}^{n} P_{re,i}}{P_{base,sys}} \cdot K_{prim} \tag{19}$$

According to (13), the total power contributed by VSD loads in p.u. value is expressed as:

$$\Delta P_{VSD,tot,pu} = K_{droop} \Delta f_{pu} \tag{20}$$

where Δf_{pu} represents the p.u. value of Δf.

According to the VSD frequency regulation expressed in (2), $P_{VSD,pu,i}$ of VSD unit i is expressed as:

$$P_{VSD,pu,i} = (\omega_{ri,ini,pu} + K_{fi} \cdot \Delta f_{pu})^3 \tag{21}$$

where K_{fi} represents K_f in i^{th} VSD unit. Considering the initial VSD unit power consumption $P_{VSD,pu,i,ini}$ is expressed as $P_{VSD,pu,i,ini} = \omega_{ri,ini,pu}^3$, so $\Delta P_{VSD,pu,i}$ is expressed as:

$$\Delta P_{VSD,pu,i} = P_{VSD,pu,i} - P_{VSD,pu,i,ini} \tag{22}$$

$$\Delta P_{VSD,pu,i} = 3\omega_{ri,ini,pu}^2 (K_{fi} \cdot \Delta f_{pu}) + 3\omega_{ri,ini,pu} (K_{fi} \cdot \Delta f_{pu})^2 + (K_{fi} \cdot \Delta f_{pu})^3 \tag{23}$$

Because we can ignore Δf_{pu} terms that are higher than first-order considering Δf_{pu} value is small, $\Delta P_{VSD,pu,i}$ can be simplified as:

$$\Delta P_{VSD,pu,i} = 3\omega_{ri,ini,pu}^2 \cdot K_{fi} \cdot \Delta f_{pu} \tag{24}$$

Accordingly, the total VSD power contribution is expressed as:

$$\Delta P_{VSD,tot,pu} = \frac{\sum_{i=1}^{n} 3K_{fi}\omega_{ri,ini,pu}^2 P_{base,i}}{P_{base,sys}} \cdot \Delta f_{pu} \tag{25}$$

Based on (25), the required K_{droop} is achieved by adjusting K_{fi} in each i^{th} VSD load unit. Substitute (13) and (25) into (20), K_{fi} is expressed regardless of Δf_{pu} direction:

$$K_{fi} = \frac{P_{re,pu,i} K_{prim}}{3\omega_{ri,ini,pu}^2 \cdot (\Delta f_{max} - \Delta f_{db})} \tag{26}$$

where $P_{re,pu,i}$ represents the reserve power of the i^{th} VSD unit in p.u. value.

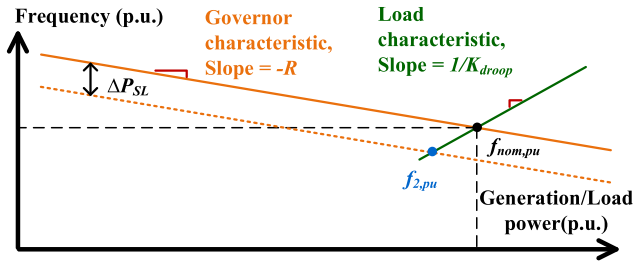

Fig. 8. Relationships between load, speed regulation and frequency.

D. Grid Frequency Deviation vs. K_{droop}

The grid frequency influenced by generator speed regulation and load response is illustrated in Fig. 8. Accordingly, both generator governor and frequency sensitive load contribute to formulating a new grid frequency after the power mismatch between generation and load occurs.

The VSD load characteristic can also be represented by proportional function regarding contributing to improving the grid frequency deviation, since the $f-p$ droop control is adopted. Reliability of Δf_{pu} can be expressed based on equivalent VSD load K_{droop}.

Assume nominal grid frequency $f_{nom,pu} = 1$, then Δf_{pu} can be expressed by $(f_{pu} - 1)$. Generation units power supply P_{SG} and load power consumption P_{Load} are expressed as:

$$P_{SG} = \Delta f_{pu} \cdot \left(\frac{-1}{R}\right) + P_{SG,pu,ini} \tag{27}$$

$$P_{Load} = \Delta f_{pu} \cdot K_{droop} + P_{VSD,pu,ini} + P_{Load,nons} \tag{28}$$

where $P_{SG,pu,ini}$ represents generation units' initial power consumption, R represents generation unit governor speed characteristic, $P_{Load,nons}$ represents loads which are non-sensitive to Δf_{pu}.

Assume generation units output power decrease by ΔP_{SL}, a new generation unit expression is formed, which is shown by the yellow dashed line in Fig. 8. So P_{SG} is updated based on (27):

$$P_{SG} = \Delta f_{pu} \cdot \left(\frac{-1}{R}\right) + P_{SG,pu,ini} - \Delta P_{SL} \tag{29}$$

Following the generation decrease ΔP_{SL}, the power grid will reach a new operating point, which is illustrated as $f_{2,pu}$ in Fig. 8. Consequently, a new grid frequency will be formed following the expression in (30), considering P_{SG} expressed in (29) equals

to P_{Load} expressed in (28):

$$\Delta f_{pu} = \frac{P_{SG,pu,ini} - \Delta P_{SL} - (P_{VSD,pu,ini} + P_{Load,nons})}{K_{droop} + \frac{1}{R}} \tag{30}$$

Considering $\Delta f_{pu} = 0$ and $P_{SG} = P_{Load}$ at nominal operating condition, the generation and load units' initial power is expressed according to (27) and (28):

$$P_{SG,pu,ini} = P_{VSD,pu,ini} + P_{Load,nons} \tag{31}$$

Substitute (31) into (30), Δf_{pu} can be expressed as:

$$\Delta f_{pu} = \frac{-\Delta P_{SL}}{K_{droop} + \frac{1}{R}} \tag{32}$$

Accordingly, a higher K_{droop} yields smaller $|\Delta f_{pu}|$.

E. VSD Load Aggregated Representation

Assuming multiple VSD load units that employ the frequency support control are located at one load center, the total power consumption $P_{VSD,tot}$ is regulated according to the VSD grid support function. Practically, Δf is measured locally by the voltage sensor of each VSD load unit. Assume the input variable Δf is identical for all VSD loads at a particular load center, and all VSD loads involved follow the same load format as illustrated in Fig. 4. Therefore, the corresponding aggregated model is equivalent to the single VSD load unit model in terms of characterizing $P_{VSD,tot}$. A numerical study will be introduced in the next section.

V. Simulation and Experimental Studies

The modeling and control of frequency responsive VSD load is further explained in the following Section A and Section B with a simulation model developed in Simulink. Section C presents experimental verification of the VSD load frequency support function.

A. Droop Response Provided by VSD Loads

An example of utilizing VSD load potential to provide $f - p$ droop control is represented below. $\omega_{ri,ini,pu}$ is selected between 79.39% and 100% $\omega_{r,nom}$, and $P_{base,i}$ is scaled as between 1 and 2 for simplification.

K_{droop} is determined based on P_{prim} provided by the VSD load group following (13). So different composition of $P_{base,i}$ and $\omega_{ri,ini,pu}$ yields different P_{prim}, thus providing different K_{droop} to the power grid.

The equivalent droop curve illustrated in Fig. 9 is based on the VSD model developed in Simulink. The blue curve represents the desired droop control, and red circles represent the VSD load frequency response. The VSD load can provide an accurate frequency response following the desired K_{droop} with the proposed frequency regulation scheme. As illustrated in Fig. 9, $K_{droop,up}$ and $K_{droop,down}$ are determined respectively by $P_{prim,up}$ and $P_{prim,down}$. In this example, $K_{droop,up} = 0.2667$ p.u./Hz and $K_{droop,down} = 0.2333$ p.u./Hz.

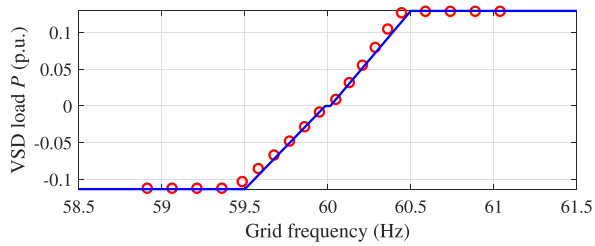

Fig. 9. VSD loads frequency response following required K_{droop}.

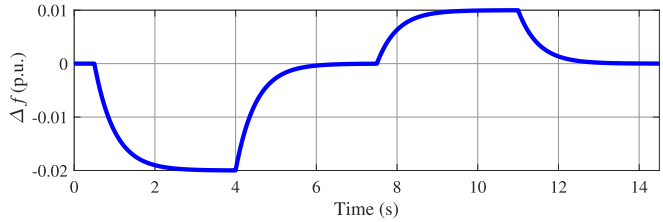

Fig. 10. Model identification input variable: Δf in p.u. value.

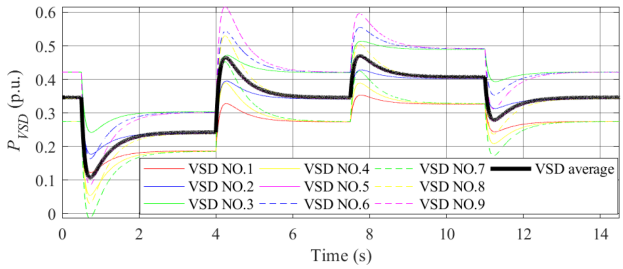

Fig. 11. VSD load power with 10 rad/s control bandwidth.

B. VSD Aggregated Model Identification Example

Two VSD load groups - each includes 9 VSD load units with different model parameters - are used to represent the aggregated performance of multiple VSD load units. An equivalent aggregated VSD load model is identified by the MATLAB system identification toolbox according to the VSD load model in Fig. 4. Input and output variables used for model identification are Δf and P_{VSD}. Δf varies with time, and P_{VSD} responds according to Δf, as illustrated in Fig. 10 and Fig. 11. The black curve in Fig. 11 represents the average power consumption $P_{VSD,agg}$ of nine VSD load units:

$$P_{VSD,agg} = \frac{\sum_{n=1}^{9}(P_{VSD,n} \cdot P_{base,n})}{\sum_{n=1}^{9} P_{base,n}} \tag{33}$$

where $P_{VSD,n}$ and $P_{base,n}$ represent the power consumption and the power base value of each VSD load unit.

Equivalent aggregated VSD load model parameters are illustrated in Fig. 4, including H_{eq}, $\omega_{r,ref,eq}$, $K_{f,eq}$, $\omega_{r,eq}$, $K_{i,eq}$, $K_{p,eq}$. Subscript eq represents "equivalent value". The VSD load state space expression in the p.u. system is expressed as follows:

$$\frac{d\Delta f}{dt} = u \tag{34}$$

Fig. 12. HTB experimental platform.

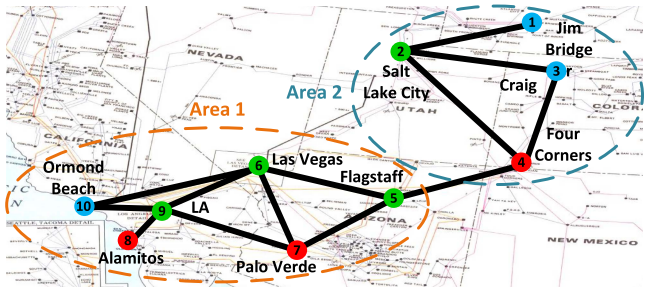

Fig. 13. Simplified southeastern area of the WECC power system.

$$\frac{dT_{e,eq}}{dt} = K_{p,eq}K_{f,eq}u - K_{p,eq}\frac{T_{e,eq} - {\omega_{r,eq}}^2}{2H_{eq}} + K_{i,eq}(K_{f,eq}\Delta f + \omega_{r,ref,eq} - \omega_{r,eq}) \quad (35)$$

$$\frac{d\omega_{r,eq}}{dt} = \frac{T_{e,eq} - {\omega_{r,eq}}^2}{2H_{eq}} \quad (36)$$

$$y = T_{e,eq} \cdot \omega_{r,eq} \quad (37)$$

where the state variables include Δf, $T_{e,eq}$ and $\omega_{r,eq}$. Additionally, input variable u is the differential of Δf, y represents the output variable $P_{VSD,agg}$.

The identification of VSD model is based on the model format in (34) to (37). The initial state space variable, and the initial estimate of model parameters can be derived by solving linearized model, (5) to (10), based on the Δf and P_{VSD} from Fig. 10 and Fig. 11. The restriction for model parameters from (34) to (37) is ≥ 0.

Normalized root mean square error (NRMSE) is adopted to quantitatively represent the model accuracy [41]. Estimated aggregated models from both groups achieve a close match compared with the actual measured output of multiple VSD devices, where the accuracy rate of group No. 1 and No. 2 are 99.81% and 99.41%, respectively.

C. VSD Grid Frequency Support Experimental Analysis

The evaluation of VSD load primary frequency support is conducted on the multi-converter-based hardware testbed (HTB) as illustrated in Fig. 12. The HTB has been developed by the Center of Ultra-wide-area Resilient Electric Energy Transmission Network (CURENT) at the University of Tennessee, which is a real power testbed featuring multiple power emulator modules based on using programmable three-phase VSCs [42]. The HTB is regarded as an advantageous experimental platform for large-scale power systems analysis considering broad time scales, less dependency on numerical calculation, capable of performing prolonged real-time experiments, and the real-power-based testing environment [28], [43], [44], [45], [46].

The experimental results are shown and explained in this section. As mentioned previously, VSD-based pump/fan loads are appropriate candidates for frequency responsive loads. Although only a small portion of this type of motor load is driven by VSDs, many more motor loads will be converted to electric drives in the near future for increased efficiency and performance as discussed in [47]. Therefore, it is reasonable to predict that a considerable number of motor loads will soon evolve to VSD loads. The VSD frequency responsive load experiments introduced in this section are based on this assumption.

TABLE I
VSD LOAD PENETRATION LEVEL

Time / Weather	4 am		10 am		4 pm		10 pm	
	case	[%]	case	[%]	case	[%]	case	[%]
Normal	1	13.13	2	8.81	3	7.5	4	9.87
Hot	5	8.46	6	5.24	7	4.17	8	5.58

1) Aggregated VSD Model Representation in HTB: The responsive VSD load model is integrated into the southeastern area of the simplified Western Electricity Coordinating Council (WECC) system to evaluate frequency support functions. The simplified WECC diagram is illustrated in Fig. 13. VSC-based power emulators mimic Bus 1 to 10 in the HTB, of which red circles represent generation buses, green circles represent load buses, and blue circles represent generation and load combined buses.

The aggregated VSD load model can be represented by the simplified model of a single VSD load unit. Considering the computational processing capability of power emulator DSP, 6 to 8 VSD load models with different model parameters are applied to one power emulator unit.

2) VSD Load Frequency Support Experimental Verification: Industrial end-use loads, such as ventilation fans or water circulation cooling pumps, can be actively controlled to provide grid frequency service. The amount of VSD load available for frequency support is the crucial factor that decides the frequency regulation impact. According to (13), a higher VSD load power reserve yields higher K_{droop} and more active power contribution for the frequency regulation. Conversely, lower VSD load power reserve yields lower K_{droop} and less active power. Industrial VSD load portion decreases with the increase of temperature, and according to the load profile in WECC during summer, 4 am has the lowest average temperature in normal summer mode, while 4 pm has the highest average temperature in the hot summer mode. So, the responsive VSD load penetration level changes based on different weather and time of day. Consequently, the overall impact of the frequency support function will vary significantly. Eight cases listed in Table I are tested to fully represent the frequency support performance at different

TABLE II
TEST POWER NETWORK LOAD DISTRIBUTION. POWER NETWORK BASE POWER = 10 GW

Bus	P (p.u.)	Bus	P (p.u.)	Bus	P (p.u.)	Bus	P (p.u.)
1	0.1	2	0.1	3	0.1	5	0.1
6	0.2	9	0.35	10	0.04		

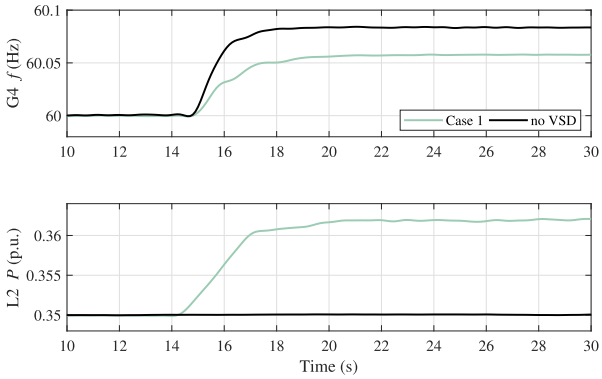

Fig. 14. Comparison between enabling and disabling VSD load support in frequency event.

operating points. The responsive VSD load is evenly applied to each load bus, *e.g.,* in case 1, the VSD load accounts for 13.13% of the total load consumption for all load buses. The power flow of each load bus is presented in Table II, where the load power p.u. value is computed based on the HTB experimental platform power base 10 GW.

First, the VSD load grid frequency support function with unequal K_{droop} is performed and analyzed. K_{droop} for each load unit is decided according to (13), so K_{droop} is different considering different P_{re} as listed in Table I. The grid frequency increase event is performed by shedding 0.08 p.u. of the total load at Bus 5, and the grid frequency decrease event is performed by tripping 0.08 p.u. of the total generation at Bus 7. G4, the generation unit at Bus 4, is selected to demonstrate the grid frequency. Meanwhile, L2, the load at Bus 2, is selected to represent the VSD load response when subject to Δf.

The comparison between cases when enabling and disabling the VSD load grid frequency support in the frequency event is presented in Fig. 14, where Case 1 is illustrated as an example. When VSD load frequency support is enabled, the Δf is smaller compared with that when support is disabled. The active power released by the VSD load to mitigate the Δf is also represented by the L2 power consumption curve. In comparison, the L2 power has no variation when the frequency support is disabled.

Similar levels of grid frequency contribution provided by VSD loads is observed when performing load shedding and generation tripping events at different buses. Experimental results from all buses are not presented considering the length of paper. Therefore, only G4 and L2 are selected to represent the grid frequency and VSD load performance in this subsection.

Next, a grid frequency increase event for Cases 1 to 8 is illustrated in Fig. 15. All represented cases demonstrate different

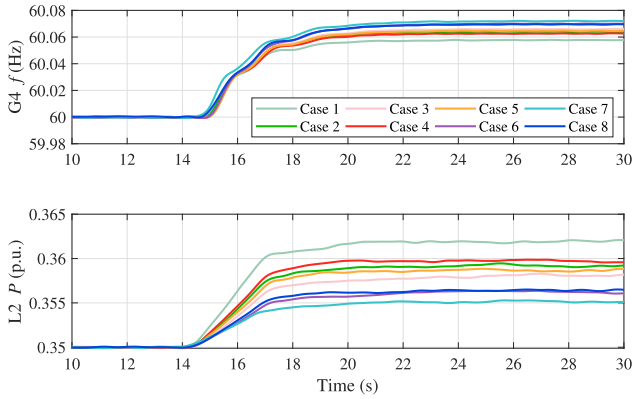

Fig. 15. VSD load providing grid frequency support in the frequency increase event with unequal K_{droop}.

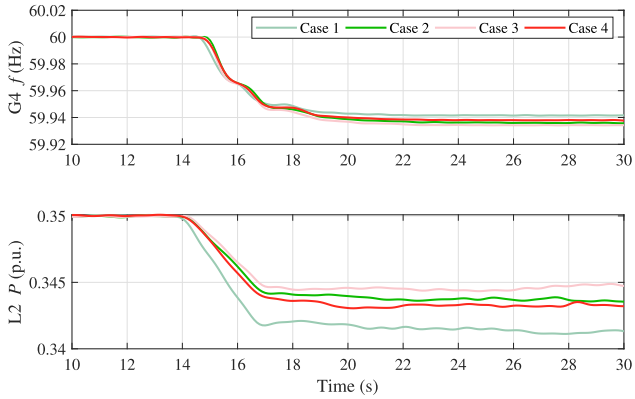

Fig. 16. VSD load providing grid frequency support in the frequency decrease event with unequal K_{droop}.

grid support potential under the same power mismatch condition. Grid frequency deviation is more significant in cases with fewer VSD loads, and less significant with more VSD loads. For example, Δf is the smallest in Case 1, and the largest in Case 7, corresponding to different load penetration levels in each case. Meanwhile, more load active power support is provided in cases with higher VSD load percentages by observing L2 experimental results.

As shown in Fig. 16, similar frequency support performance is observed in the grid frequency decrease event: in cases that have higher VSD load penetration level, more active power support is provided to mitigate the generation and load power mismatch, thus yields less Δf. Fig. 16 only includes experimental results from Case 1 to 4, since the trend is similar for the remaining 4 cases.

Furthermore, the VSD load grid frequency support function with equal K_{droop} is also investigated. Although equal K_{droop} is applied, the grid support performance may vary due to different VSD load penetration levels. Experimental results comparison for frequency increase event between Case 4 and Case 8 is illustrated in Fig. 17. When $K_{droop} = 20$ p.u./Hz, the grid frequency response of each load is very similar since the required active

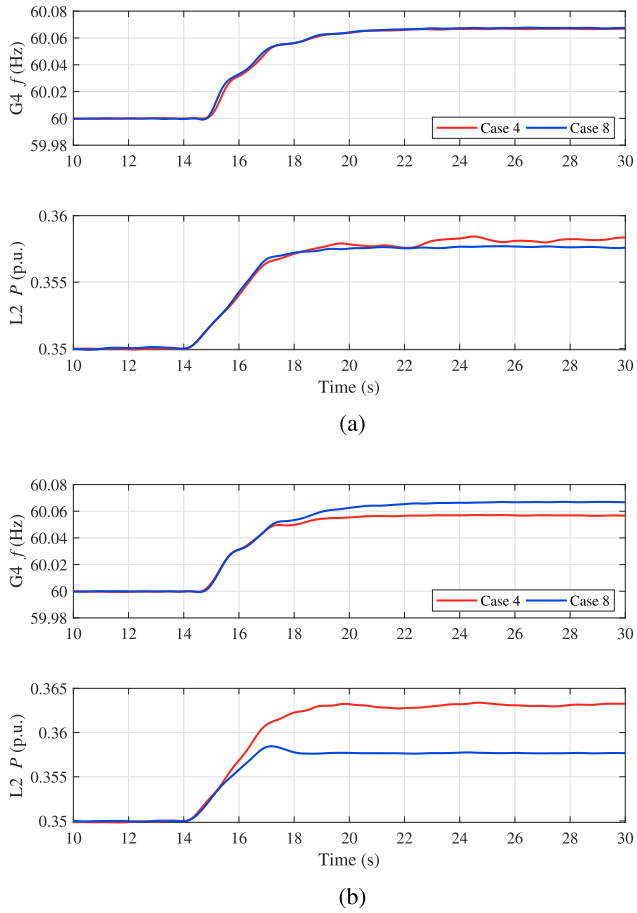

Fig. 17. VSD load providing grid frequency support in the frequency increase event with equal K_{droop}. (a) $K_{droop} = 20$ p.u./Hz. (b) $K_{droop} = 40$ p.u./Hz.

power contribution can be provided in each case, so similar grid frequency performance is observed in Fig. 17(a).

In comparison, if increasing K_{droop} to 40 p.u./Hz, the required active power support cannot be entirely provided by Case 8 considering the limited VSD load power reserve. So a significant grid frequency and power difference are observed between Case 4 and Case 8 in Fig. 17(b). In conclusion, the VSD load power reserve limit varies considering different operating points, leading to different impacts to the grid even with identical K_{droop} command. Therefore, the frequency support decision should be effectively made considering the impact of a responsive load amount, *i.e.,* a large K_{droop} can be satisfied when load power reserve is sufficient, and K_{droop} should be decreased appropriately when the load reserve is limited.

VI. Conclusion

In this paper, non-critical VSD-driven fan/pump loads are utilized to provide grid frequency support based on the proposed load frequency regulation scheme. Additionally, the VSD load model is simplified and aggregated to characterize the overall dynamic performance of multiple VSD load units, which maintains a good balance between accuracy and simplicity. Meanwhile, the potential of VSD load grid support is also investigated, where the $f - p$ droop response can be provided by coordinating multiple VSD load units.

Experiments for evaluating the VSD load grid frequency response have been performed in a hardware testbed, and the experimental results show that the VSD load can effectively mitigate the grid frequency deviation if operating within the total load power reserve. Meanwhile, droop control coefficient K_{droop} is determined according to the power grid operating point, which is significantly influenced by the time of day and weather. Experimental results show that the available VSD load power reserve level leads to varied frequency support performance even with identical K_{droop} command.

References

[1] Energy Information Administration, "Annual energy outlook 2020," Jan. 2020. [Online]. Available: https://www.eia.gov/outlooks/aeo/
[2] F. Blaabjerg, R. Teodorescu, M. Liserre, and A. V. Timbus, "Overview of control and grid synchronization for distributed power generation systems," *IEEE Trans. Ind. Electron.*, vol. 53, no. 5, pp. 1398–1409, Oct. 2006.
[3] J. M. Carrasco et al., "Power-electronic systems for the grid integration of renewable energy sources: A survey," *IEEE Trans. Ind. Electron.*, vol. 53, no. 4, pp. 1002–1016, Jun. 2006.
[4] W. Su, J. Wang, and J. Roh, "Stochastic energy scheduling in microgrids with intermittent renewable energy resources," *IEEE Trans. Smart Grid*, vol. 5, no. 4, pp. 1876–1883, Jul. 2014.
[5] National Grid Electricity Transmission, "The grid code," Mar. 2017. [Online]. Available: https://www.nationalgrid.com/sites/default/files/documents/8589935310-Complete%20Grid%20Code.pdf
[6] S. Yan, S.-C. Tan, C.-K. Lee, B. Chaudhuri, and S. R. Hui, "Electric springs for reducing power imbalance in three-phase power systems," *IEEE Trans. Power Electron.*, vol. 30, no. 7, pp. 3601–3609, Jul. 2015.
[7] S.-C. Tan, C. K. Lee, and S. Hui, "General steady-state analysis and control principle of electric springs with active and reactive power compensations," *IEEE Trans. Power Electron.*, vol. 28, no. 8, pp. 3958–3969, Aug. 2013.
[8] D. Mao, K. Potty, and J. Wang, "The impact of power-electronics-based load dynamics on large-disturbance voltage stability," in *Proc. IEEE Power Energy Soc. Gen. Meeting*, 2018, pp. 1–5.
[9] U. Datta, A. Kalam, and J. Shi, "Battery energy storage system to stabilize transient voltage and frequency and enhance power export capability," *IEEE Trans. Power Syst.*, vol. 34, no. 3, pp. 1845–1857, May 2019.
[10] G. Meng et al., "Energy storage auxiliary frequency modulation control strategy considering ACE and SOC of energy storage," *IEEE Access*, vol. 9, pp. 26271–26277, 2021.
[11] S. G. Mian, P. D. Judge, A. Junyent-Ferŕ, and T. C. Green, "A delta-connected modular multilevel STATCOM with partially-rated energy storage for provision of ancillary services," *IEEE Trans. Power Del.*, vol. 36, no. 5, pp. 2893–2903, Oct. 2021.
[12] P. D. Judge and T. C. Green, "Modular multilevel converter with partially rated integrated energy storage suitable for frequency support and ancillary service provision," *IEEE Trans. Power Del.*, vol. 34, no. 1, pp. 208–219, Feb. 2019.
[13] C. K. Lee and S. Y. Hui, "Reduction of energy storage requirements in future smart grid using electric springs," *IEEE Trans. Smart Grid*, vol. 4, no. 3, pp. 1282–1288, Sep. 2013.
[14] D. Mao, H. J. Khasawneh, M. S. Illindala, B. L. Schenkman, and D. R. Borneo, "Economic evaluation of energy storage options in a microgrid with flexible distribution of energy and storage resources," in *Proc. IEEE Ind. Commercial Power Syst. Tech. Conf.*, 2015, pp. 1–7.
[15] Y. Liu et al., "Open-source high-fidelity aggregate composite load models of emerging load behaviors for large-sale analysis," Pacific Northwest Nat. Lab. (PNNL), Richland, WA, USA, Tech. Rep. PNNL-29592, 2020.
[16] Z. Akhtar, B. Chaudhuri, and S. Y. R. Hui, "Primary frequency control contribution from smart loads using reactive compensation," *IEEE Trans. Smart Grid*, vol. 6, no. 5, pp. 2356–2365, Sep. 2015.
[17] T. Chen, H. Liu, C.-K. Lee, and S. R. Hui, "A generalized controller for electric-spring-based smart load with both active and reactive power compensation," *IEEE Trans. Emerg. Sel. Topics Power Electron.*, vol. 8, no. 2, pp. 1454–1465, Jun. 2020.

[18] X. Luo, C. K. Lee, W. M. Ng, S. Yan, B. Chaudhuri, and S. Y. R. Hui, "Use of adaptive thermal storage system as smart load for voltage control and demand response," *IEEE Trans. Smart Grid*, vol. 8, no. 3, pp. 1231–1241, May 2017.
[19] Q. Shi, F. Li, G. Liu, D. Shi, Z. Yi, and Z. Wang, "Thermostatic load control for system frequency regulation considering daily demand profile and progressive recovery," *IEEE Trans. Smart Grid*, vol. 10, no. 6, pp. 6259–6270, Nov. 2019.
[20] A. Molina-Garcia, F. Bouffard, and D. S. Kirschen, "Decentralized demand-side contribution to primary frequency control," *IEEE Trans. Power Syst.*, vol. 26, no. 1, pp. 411–419, Feb. 2011.
[21] K. Kalsi et al., "Loads as a resource: Frequency responsive demand," Pacific Northwest Nat. Lab. (PNNL), Richland, WA, USA, Tech. Rep. PNNL-25397, 2015.
[22] K. Kalsi, W. Zhang, J. Lian, L. D. Marinovici, C. Moya, and J. E. Dagle, "Distributed smart grid asset control strategies for providing ancillary services," Pacific Northwest Nat. Lab. (PNNL), Richland, WA, USA, Tech. Rep. PNNL-22875, 2013.
[23] R. Azizipanah-Abarghooee and M. Malekpour, "Smart induction motor variable frequency drives for primary frequency regulation," *IEEE Trans. Energy Convers.*, vol. 35, no. 1, pp. 1–10, Mar. 2020.
[24] J. Carmona-Sánchez, M. Barnes, and J. M. Apsley, "Virtual energy storage: Converting an AC drive to a smart load," *IEEE Trans. Energy Convers.*, vol. 33, no. 3, pp. 1342–1353, Sep. 2018.
[25] M. Malekpour, R. Azizipanah-Abarghooee, F. Teng, G. Strbac, and V. Terzija, "Fast frequency response from smart induction motor variable speed drives," *IEEE Trans. Power Syst.*, vol. 35, no. 2, pp. 997–1008, Mar. 2020.
[26] S. Wang, Y. Ma, J. Wang, L. M. Tolbert, and F. Wang, "Variable speed drive connected motor load emulator for a multi-converter-based hardware testbed system," *IEEE Open J. Ind. Appl.*, vol. 2, pp. 337–346, 2021.
[27] T. L. Short et al., "Primary frequency control using motor drives for short term grid disturbances," *IEEE Open J. Ind. Appl.*, vol. 2, pp. 1–10, 2021.
[28] W. Cao et al., "Two-stage PV inverter system emulator in converter based power grid emulation system," in *Proc. IEEE Energy Convers. Congr. Expo.*, 2013, pp. 4518–4525.
[29] X. Shi, Z. Wang, Y. Ma, L. Hang, L. M. Tolbert, and F. Wang, "Modeling and control of an LCL filter based three-phase active rectifier in grid emulator," in *Proc. IEEE 28th Annu. Appl. Power Electron. Conf. Expo.*, 2013, pp. 992–998.
[30] P. C. Krause, O. Wasynczuk, S. D. Sudhoff, and S. Pekarek, *Analysis of Electric Machinery and Drive Systems*, 2nd ed. Hoboken, NJ, USA: Wiley, 2002.
[31] U. S. Department of Energy, Nov. 2012. [Online]. Available: "Adjustable speed drive part-load efficiency," https://www.energy.gov/sites/prod/files/2014/04/f15/motor_tip_sheet11.pdf
[32] U.S. Department of Energy, "Determining electric motor load and efficiency," Apr. 2014. [Online]. Available: https://www.energy.gov/sites/prod/files/2014/04/f15/10097517.pdf
[33] H. Liu and Z. Chen, "Contribution of VSC-HVDC to frequency regulation of power systems with offshore wind generation," *IEEE Trans. Energy Convers.*, vol. 30, no. 3, pp. 918–926, 2015.
[34] F. Gonzalez-Longatt, "Frequency control and inertial response schemes for the future power networks," in *Large Scale Renewable Power Generation*. Berlin, Germany: Springer, 2014, pp. 193–231.
[35] R. K. Subroto, K. L. Lian, C.-C. Chu, and C.-J. Liao, "A fast frequency control based on model predictive control taking into account of optimal allocation of power from the energy storage system," *IEEE Trans. Power Del.*, vol. 36, no. 4, pp. 2467–2478, Aug. 2021.
[36] A. Kirakosyan, E. F. El-Saadany, M. S. E. Moursi, and K. Al Hosani, "DC voltage regulation and frequency support in pilot voltage droop-controlled multiterminal HVdc systems," *IEEE Trans. Power Del.*, vol. 33, no. 3, pp. 1153–1164, Jun. 2018.
[37] M. Langwasser, G. De Carne, M. Liserre, and M. Biskoping, "Primary frequency regulation using HVDC terminals controlling voltage dependent loads," *IEEE Trans. Power Del.*, vol. 36, no. 2, pp. 710–720, Apr. 2021.
[38] J. L. Jorgenson and P. L. Denholm, "Modeling primary frequency response for grid studies," Nat. Renewable Energy Lab. (NREL), Golden, CO, USA, Tech. Rep. NREL/TP-6A20-72355, 2019.
[39] M. Brown, "Siemens standard drives application handbook," Dec. 1997. [Online]. Available: https://cache.industry.siemens.com/dl/files/430/1160430/att_36835/v1/applications_e.pdf
[40] V. Vodovozov, L. Gevorkov, and Z. Raud, "Circulation centrifugal pump with variable speed drives and minimal electricity consumption," in *Proc. IEEE 11th Int. Conf. Compat., Power Electron. Power Eng.*, 2017, pp. 334–339.
[41] Saskia, "How to normalize the RMSE," Jan. 2019. [Online]. Available: https://www.marinedatascience.co/blog/2019/01/07/normalizing-the-rmse/
[42] L. Yang et al., "Development of converter based reconfigurable power grid emulator," in *Proc. IEEE Energy Convers. Congr. Expo.*, 2014, pp. 3990–3997.
[43] J. Wang, "Versatile three-phase power electronics converter based real-time load emulators," Ph.D. dissertation, The University of Tennessee, Knoxville, TN, USA, 2015.
[44] S. Zhang, B. Liu, S. Zheng, Y. Ma, F. Wang, and L. M. Tolbert, "Development of a converter-based transmission line emulator with three-phase short-circuit fault emulation capability," *IEEE Trans. Power Electron.*, vol. 33, no. 12, pp. 10215–10228, Dec. 2018.
[45] J. Wang et al., "Static and dynamic power system load emulation in a converter-based reconfigurable power grid emulator," *IEEE Trans. Power Electron.*, vol. 31, no. 4, pp. 3239–3251, Apr. 2016.
[46] S. Wang, H. Li, J. Wang, Y. Ma, F. Wang, and L. M. Tolbert, "A power converter based real-time air-conditioner motor emulator," in *Proc. IEEE Appl. Power Electron. Conf. Expo.*, 2020, pp. 70–76.
[47] WECC Significant Electrification Task Force, "WECC significant electrification task force update," Oct. 2019. Accessed: Jul. 8, 2020. [Online]. Available: https://www.wecc.org/Administrative/Melloni%20-%20Significnat%20Electrification.pdf

Shuyao Wang (Member, IEEE) received the B.S. and M.S. degrees in electrical engineering from North China Electric Power University, Beijing, China, in 2013 and 2016, respectively, and the Ph.D. degree in electrical engineering from the University of Tennessee, Knoxville, TN, USA, in 2021. She is currently a Senior Applications Engineer with Monolithic Power Systems, Inc., San Jose, CA, USA. Her research interests include modular multilevel converters, HVDC transmission system, power grid ancillary services, and power electronics based devices modeling.

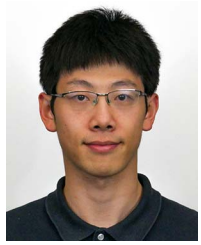

Yiwei Ma (Member, IEEE) received the B.S. and M.S. degrees in electrical engineering from Tsinghua University, Beijing, China, in 2009 and 2011, respectively, and the Ph.D. degree in electrical engineering from the University of Tennessee, Knoxville, TN, USA, in 2019. He is currently a Research Engineer with Electric Power Research Institute, Knoxville, TN, USA. His research interests include modeling and control of power electronics interfacing converters for the renewable energy sources, multilevel converters, and microgrids.

Kaiqi Sun (Member, IEEE) received the B.S. and Ph.D. degree in electrical engineering from Shandong University, Jinan, China, in 2015 and 2020, respectively. From 2017 to 2020, he was also a Visiting Scholar with the University of Tennessee, Knoxville, TN, USA. From 2020 to 2021, he was a Research Associate with the Department of Electrical Engineering and Computer Science, University of Tennessee. He is currently an Associate Research Fellow with Shandong University. His research interests include the HVDC and MVDC system operation, renewable energy integration, and machine learning based power system application.

Jingxin Wang (Member, IEEE) received the B.S. and M.S. degrees in electrical engineering from the China University of Mining and Technology, Xuzhou, China, 2003 and 2006, respectively, and the Ph.D. degree in electrical engineering from Shanghai Jiao Tong University, Shanghai, China, in 2011. He is currently a Research Associate with the University of Tennessee, Knoxville, TN, USA. His research interests include high performance motor control, three-phase converter design, power flow control, and renewable energy.

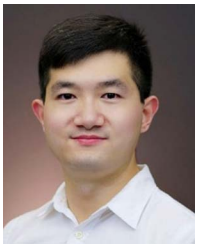

Hongyu Li (Student Member, IEEE) received the B.S. and Ph.D. degree in electrical engineering in 2012 and 2018, respectively. He is currently a Research Assistant with the University of Tennessee, Knoxville, TN, USA. His main research interests include power system dynamics under stochastic disturbances and situation awareness for power system frequency dynamics.

Leon M. Tolbert (Fellow, IEEE) received the bachelor's, M.S., and Ph.D. degrees in electrical engineering from the Georgia Institute of Technology, Atlanta, GA, USA, in 1989, 1991, and 1999, respectively. He is currently a Chancellor's Professor and the Min H. Kao Professor with the Department of Electrical Engineering and Computer Science, University of Tennessee, Knoxville, TN, USA. He is a Founding Member for the NSF/DOE Engineering Research Center, Center for Ultra-wide-area Resilient Electric Energy Transmission Networks (CURENT). He is also an Adjunct Participant with Oak Ridge National Laboratory, Oak Ridge, TN, USA. His research interests include the utility applications of power electronics, microgrids, electric vehicles, and wide bandgap semiconductors. He is a Registered Professional Engineer with the State of Tennessee.

Fei (Fred) Wang (Fellow, IEEE) received the B.S. degree in electrical engineering from Xi'an Jiaotong University, Xi'an, China, in 1982, and the M.S. and Ph.D. degrees in electrical engineering from the University of Southern California, Los Angeles, CA, USA, in 1985 and 1990, respectively. From 1990 to 1992, he was a Research Scientist with the Electric Power Lab, University of Southern California. In 1992, he joined GE Power Systems Engineering Department, Schenectady, NY, USA, as an Application Engineer. From 1994 to 2000, he was a Senior Product Development Engineer with GE Industrial Systems, Salem, VA, USA. From 2000 to 2001, he was the Manager of Electronic and Photonic Systems Technology Lab, GE Global Research Center, Schenectady, NY, USA, and Shanghai, China. In 2001, he joined Center for Power Electronics Systems at Virginia Tech, Blacksburg, VA, USA, as a Research Associate Professor and became an Associate Professor in 2004. From 2003 to 2009, he was also the CPES Technical Director. Since 2009, he has been with The University of Tennessee and Oak Ridge National Lab, Knoxville, TN, USA, as a Professor and the Condra Chair of Excellence in Power Electronics. His research interests include wide bandgap power electronics, power electronics applications for transportation, and electric grid. He is a Fellow of the U.S. National Academy of Inventors.